Tectonophysics, 95 (1983) 133–156
Elsevier Science Publishers B.V., Amsterdam – Printed in The Netherlands

FAULTING OF ROCKS IN THREE-DIMENSIONAL STRAIN FIELDS II. THEORETICAL ANALYSIS

ZE'EV RECHES

Department of Applied Mathematics, The Weizmann Institute of Science, Rehovot (Israel) *

(Received January 22, 1982; revised version accepted September 2, 1982)

ABSTRACT

Reches, Z., 1983. Faulting of rocks in three-dimensional strain fields. II. Theoretical analysis. *Tectonophysics*, 95: 133–156.

The model for the faulting of rocks in a three-dimensional strain field is derived here. It is assumed that the strain applied on a rock is accommodated by slip along faults. It is shown that four sets of faults in orthorhombic symmetry are required to accommodate general, three-dimensional deformation. It is further assumed that the preferred faults, namely, those which are most likely to slip, require the minimum stress difference and minimum dissipation. The orientations of these theoretically preferred faults are derived, and are compared with the experimental results of Part I (Reches and Dieterich, 1983). Good agreement is found between the predicted and observed orientations of faults in the Berea sandstone and Candoro limestone, whereas, faults in granites deviate from the predicted orientations. Good agreement is also found between predicted and observed stresses of all experiments. Charts of the preferred faults predicted by the present model are given in an Appendix.

INTRODUCTION

The faulting of rocks is usually analyzed by two different approaches. In the first approach, a *yield criterion* is either postulated or determined experimentally, whereas in the second approach, the *mechanism* of yielding is initially postulated and the yielding stresses are then derived. The first approach incorporates criteria such as maximum shear stress (Tresca's criterion), maximum octahedral shear stress, Von Mises' criterion and a series of empirical criteria (e.g. Paterson, 1978). The Coulomb criterion, applied by Anderson (1951) to faulting of rocks, also belongs to this approach. The second approach includes Griffith's model, models which assumed slip on preexisting faults (e.g. Jaeger and Cook, 1969) or interference between faults (Oertel, 1965). The primary objective of most models is to determine the states of

* Present address: Department of Geology, Hebrew University, Jerusalem (Israel).

0040-1951/83/$03.00

stress which cause the yielding of rocks. Models using both approaches predict the development of a conjugate set of faults, which intersect parallel to the intermediate stress axis and have no slip component in the direction of this axis (e.g. Anderson, 1951). Therefore, these models imply no strain due to slip along faults in the direction of the intermediate axis. The strain associated with the faulting is therefore plane strain.

A different model of faulting is presented here. In this model *the accommodation of strain by slip along preexisting faults* is analyzed. It is assumed that this slip is the sole means of deformation and that the resistance to slip along the faults is both cohesive and frictional. It is further assumed that the faults which accommodate the applied strain with minimum dissipation are the ones most likely to slip. This model, termed here the "*slip model*", belongs to the second group of faulting models described above. At the present state, the "slip model" is derived for preexisting faults and thus, may not be directly applied to yielding of an unfaulted sample.

The development of the "slip model" resulted from the experimental observations of Oertel (1965) and the field data of Aydin (1977). In both cases they recognized four sets of penecontemporaneous faults in orthorhombic symmetry; none of which could be considered a conjugate set. Oertel (1965) clearly demonstrated that a three-dimensional state of strain prevailed in his experiments, suggesting that the observed orthorhombic pattern is due to the general strain conditions. Aydin (1977) documented patterns of three or four contemporaneous sets of faults in the Entrada and Navajo sandstones, Utah. He suggested that these orthorhombic patterns can be interpreted as slip surfaces derived by the theory of plasticity for three-dimensional strain (Aydin, pers. commun., 1977). Reches (1978) presented a slip model in which the strain is accommodated by slip along faults with only cohesive resistance to shear. He showed that the development of four sets of faults with orthorhombic symmetry occurs in a three-dimensional strain field whereas two sets of faults with a conjugate pattern, arise as a result of plane strain. These patterns are independent of the properties of the faulted material. This simple model lacks frictional resistance to slip, which is common for most rocks. The present model on the other hand, does include such resistance.

Experiments investigating the failure of rocks are usually conducted under axisymmetric strain or plane strain. However, according to Oertel (1965), Aydin (1977), and Reches (1978), the othorhombic fault patterns develop under general three-dimensional strain. Therefore, we (Reches and Dieterich, Part I) have run a series of experiments under general three-dimensional strain, using a servo-controlled apparatus. In this paper the main results of these experiments will be compared with the predictions of the "slip model".

As there is no reason to believe that in the field rocks are faulted under plane or axisymmetric strain, it is proposed here that the "slip model" should be applied to both field and experimental results.

THEORETICAL ANALYSIS OF THE "SLIP MODEL"

The deformation of a medium due to slip along faults is analyzed here in several steps. First, the properties of the idealized model and the symplifying assumptions are outlined. Then, the geometry of the faults, the strain field and the stress field are derived. Finally, the orientations of the preferred faults are determined.

The idealized model has the following properties:

(1) The model contains many surfaces of discontinuity with random orientation, prior to the deformation.

(2) The applied deformation is accommodated solely by slip along a few sets of faults selected from the preexisting surfaces of discontinuity. It is assumed that the selected sets require the minimum dissipation to maintain slip under a given strain.

(3) There is a sufficient density of faults in each set, such that the deformation of a rock containing the faults can be considered as approximately homogeneous.

(4) The resistance to slip along the faults obeys Coulomb's friction law and therefore has both cohesive and frictional components.

The idealized model is similar to that presented by Reches (1978), except that *frictional* resistance is now included. The analysis is for infinitesimal strains. Thus elastic, viscous or plastic deformation may be superimposed. Homogeneous stress distribution and coincidence of stress and strain axes are assumed.

The slip along many faults *within* a set, generates *simple shear* within the coordinate system of this set (Oertel, 1965; Reches, 1978). The superposition of the simple shears along several sets, generates three-dimensional deformation in the coordinate system of the model. The contribution of each set of faults to the general deformation can be calculated by transformation from the coordinate system of the set, to the general coordinates. As coordinates of a set of faults three mutually perpendicular axes were chosen: x_1 is normal to the set and the two slip axes, x_2 and x_3 are within the set. As the shear in the x_2 direction is independent of the shear in the x_3 direction, each set of faults has *two* independent shear contributions to the general deformation (Reches, 1978).

As in strain accommodation within crystals (e.g. Taylor, 1938), the required number of independent contributions of shears equals the number of independent components in the strain and rotation tensors. The strain tensor, $\boldsymbol{e}_{ij}$, for three dimensions has six independent components, whereas the rotation tensor, $\boldsymbol{\omega}_{ij}$, has three such components. As slip along faults is the sole deformation mechanism, there is no volume change, and the strain tensor includes only five independent components.

Therefore, three sets of faults, each of them with two independent contributions of shear, are necessary and sufficient to accommodate three-dimensional strain. If, however, a specified rotation field is applied to the model in addition to a specified strain field, *four sets* of faults are necessary and sufficient to accommodate the eight independent components of both tensors (Reches, 1978).

The three or four sets of faults required to accommodate the deformation may have arbitrary orientations with respect to the principal strain axes. We assume, however, that faults with certain orientations are more "efficient" than faults with other orientations. (This efficiency will be defined later.). As the strain field has orthorhombic symmetry, every "efficient" fault has three additional faults, generated by the orthorhombic symmetry operations, which carry the same contributions to the principal strains e_1, e_2 and e_3 (Fig. 1). For example, consider a fault I, the normal to which has N_1, N_2 and N_3 (all non-negative) as the direction cosines with respect to the three principal axes X_1, X_2 and X_3 respectively. Here $N_i = \cos(\theta_{i,N})$, $i = 1, 2, 3$ (Fig. 2). The orthorhombic symmetry generates faults II with N_1, $-N_2$ and N_3 as directional cosines of the normal, and similarly, fault III with $-N_1$, $-N_2$ and N_3 and fault IV with $-N_1$, N_2 and N_3 and the corresponding slip directions (eq. 1 below). According to eq. 1 below, all these four faults have the same coefficients N_iS_j (eq. 2a below), and thus, make the same relative contributions to the principal strains. It appears that all these four faults sets have the same "efficiency" with respect to the principal strains. They are therefore, equivalent and should shear in equal amounts simultaneously.

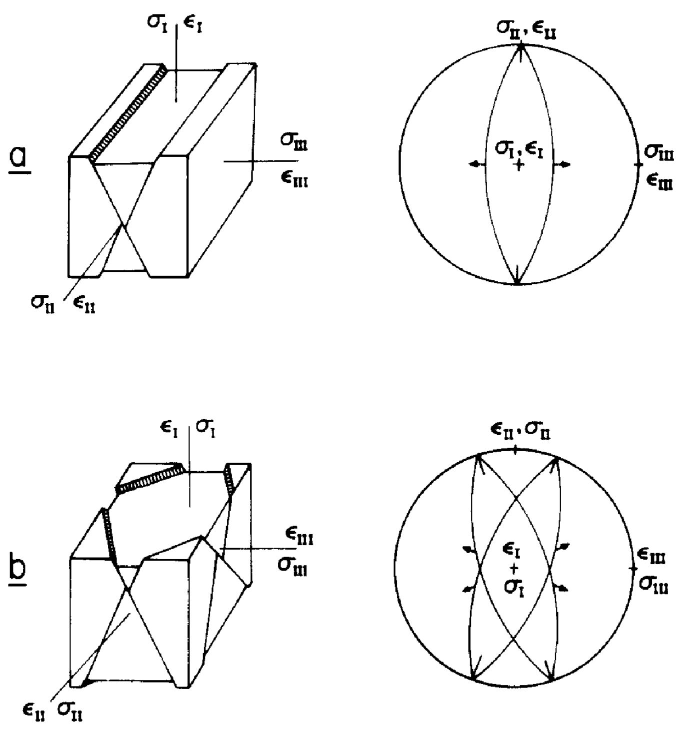

Fig. 1. a A conjugate set of normal faults, and the associated principal stress and strain axes according to Anderson (1951).
b. Four sets of normal faults that can accommodate three-dimensional strain, and the orientations of the principal stress and strain axes. Arrows indicate slip directions in both diagrams.

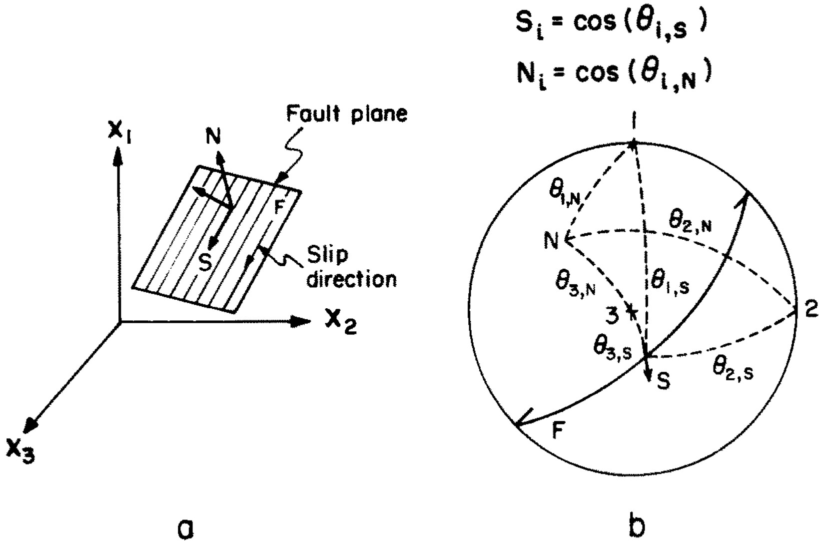

Fig. 2. a. The orientation of a fault plane with respect to the coordinate system of the principal strain axes. The strain axes are marked X_1, X_2 and X_3; the normal to the fault and the slip direction on it, are marked N and S respectively.
b. Stereographic projection of the angular relationship shown in Fig. 2a. Lower hemisphere, Wulff net.

In conclusion, it is shown by symmetry arguments, that the four sets required to accommodate the deformation, are arranged in orthorhombic symmetry with respect to the principal deformation axes.

The strain field

The geometry of the four sets of faults in the idealized model is shown in Fig. 1b. due to the orthorhombic symmetry the direction cosines may be written as follows:

Fault I: N_1, N_2 and N_3; S_1, S_2 and S_3

Fault II: N_1, $-N_2$ and N_3; S_1, $-S_2$ and S_3

Fault III: $-N_1$, $-N_2$ and N_3; $-S_1$, $-S_2$ and S_3

Fault IV: $-N_1$, N_2 and N_3; $-S_1$, S_2 and S_3 (1)

where N_i and S_i ($i = 1, 2, 3$) are the absolute values of the direction cosines of the normal to the fault set and set and of the corresponding slip direction with respect to the principal axes (Fig. 2). One can show that due to eq. 1 the contributions of all four sets may be represented by a *single* set, for example fault I (Reches, 1978, App. II).

The deformation tensor is $\boldsymbol{d}_{ij} = \partial u_i / \partial x_j$, $i, j = 1, 2, 3$, where u_i are the displacements. In the coordinate system of fault I we get

$$\boldsymbol{d}_{ij} = {}^{\mathrm{I}}\gamma \begin{bmatrix} 0 & 0 & 0 \\ 0 & 0 & 0 \\ 1 & 0 & 0 \end{bmatrix} \qquad (2)$$

where ${}^{\mathrm{I}}\gamma$ is the simple shear associated with the slip along set I (Reches, 1978). For simplicity we choose the coordinate system of fault I [Eq. (1)] so that the slip in the x_2 direction vanishes [Eq. (2)]. The fault set appears therefore, as one slip system. Any other choice of coordinates will reveal the second slip system. The deformation in the coordinate system of set I, can be transformed to the principal axes by:

$$ {}^{\mathrm{I}}\boldsymbol{D}_{ij} = N_i S_j {}^{\mathrm{I}}\gamma, \qquad i, j = 1, 2, 3 \tag{2a} $$

where ${}^{\mathrm{I}}\boldsymbol{D}_{ij}$ is the contribution of set I to the total deformation D_{ij}.

The total strain tensor due to equal slip along the four sets (eq. 1). using eqs. 2 is (Reches, 1978, eq. A12):

$$ \boldsymbol{D}_{ij} = 4\gamma \begin{bmatrix} N_1 S_1 & 0 & 0 \\ 0 & N_2 S_2 & 0 \\ 0 & 0 & N_3 S_3 \end{bmatrix}, \qquad i, j = 1, 2, 3 \tag{3} $$

where γ is the amount of simple shear associated with the slip along one set. Note that equal shears on four sets in orthorhombic symmetry, assure that rotations and shears along the principal planes vanish. Thus the strain tensor $\boldsymbol{e}_{ij}$ is identical to the deformation tensor $\boldsymbol{D}_{ij}$ (eq. 3). The sole deformation mechanism is slip along faults, so the slip axis must be *in* the fault plane (Fig. 2). This implies that the slip axis, S_i, is perpendicular to the normal of the fault N_i, or:

$$ N_1 S_1 + N_2 S_2 + N_3 S_3 = 0. \tag{4a} $$

As eq. 4a is the trace of the strain tensor (eq. 3), it implies *no volume change* during deformation. We further know that the direction cosines obey the relations:

$$ N_1^2 + N_2^2 + N_3^2 = 1 \tag{4b} $$

and:

$$ S_1^2 + S_2^2 + S_3^2 = 1 \tag{4c} $$

Finally, if we define a strain ratio, $k = e_2/e_1$, between the intermediate compressive strain, e_2, and maximum compressive strain, e_1, we get from eq. 3:

$$ kN_1 S_1 - N_2 S_2 = 0 \tag{4d} $$

The four eqs. 4a, 4b, 4c, and 4d indicate that, for a given strain ratio k, only two out of the six directional cosines, S_i and N_i, are independent. For example, by choosing N_1 and N_2 as independent, we obtain:

$$ S_1 = \pm \left[\frac{1 - N_1^2 + N_2^2}{1 - N_2^2 + N_1^2 \left(k^2 \dfrac{1 - N_1^2}{N_2^2} + 2k \right)} \right]^{1/2} \tag{5} $$

and the other parameters can be easily derived from eqs. 4 and 5. Thus, the orientation of the fault, N_1 and N_2 (Fig. 2), for a given strain ratio, k, determines also the slip direction on that fault.

The stress field

The slip along faults requires certain stresses to overcome the cohesion and friction of the faults. We assume that the principal stress axes coincide with the principal strain axes for the idealized model. For a preexisting fault (property 1 above) the resistance to slip (property 4 above) is:

$$\tau_R = C + \tan \phi \sigma_n \tag{6}$$

where τ_R is the shear strength resisting the slip, ϕ is the angle of friction and σ_n is the normal stress applied across the fault plane. Here, the term C refers to resistance to slip which is independent of the normal stress. During faulting the shear stress parallel to the slip direction, τ_S, is equal to the resisting strength:

$$\tau_S = \tau_R \tag{7}$$

Using transformation laws of stresses (e.g. Jaeger and Cook, 1969, p. 49), the shear and normal stresses applied on fault I [eq. 1] are:

$$\tau_S = \sigma_1 N_1 S_1 + \sigma_2 N_2 S_2 + \sigma_3 N_3 S_3 \tag{8a}$$

and:

$$\sigma_n = \sigma_1 N_1^2 + \sigma_2 N_2^2 + \sigma_3 N_3^2 \tag{8b}$$

where σ_1, σ_2 and σ_3 are the maximum, intermediate and least compressive stresses, respectively (Fig. 2). By substituting eqs. 7 and 8 into eq. 6, and by using eqs. 4 and 5, we get:

$$(\sigma_1 - \sigma_3)(N_1 S_1 - \tan \phi N_1^2) + (\sigma_2 - \sigma_3)(k N_1 S_1 - \tan \phi N_2^2) = \bar{C} \tag{9}$$

where $\bar{C} = C + \tan \phi \sigma_3$. Equation (9) has a form $f(\sigma_1, \sigma_2, \sigma_3, k) = 0$ which is similar to $f(\sigma_1, \sigma_2, \sigma_3) = 0$, the general form of criteria of failure (e.g. Jaeger and Cook, 1969, chapter 4, 6). However, eq. 9 is not a failure criterion. It is a *slip criterion*. Failure criteria specify the state of stress necessary to *initiate macroscopic faults* or fractures in an intact rock, whereas eq. 9 specifies the state of stress necessary *to accommodate a given strain by slip* along preexisting faults. Failure criteria relate to pre-yielding conditions, whereas eq. 9 relates to post-yielding conditions.

The dissipation

We assumed above (property 2) that slip should initiate along sets of preexisting faults which require the minimum dissipation. The dissipation per unit volume, w, required to maintain slip along a set of faults is:

$$w = \tau \cdot \gamma \tag{10}$$

where τ is the shear stress in the shear direction, and γ is the simple shear associated with the set (Reches, 1978, App. I). Equation (3) indicates that the cumulative shear along four sets in orthorhombic symmetry is:

$$\gamma = \frac{e_1}{4N_1S_1} \tag{11}$$

where e_1 is the maximum compressive strain in the general coordinates. Substituting eqs. 4a, 4d, 8a and 11 into eq. 10 yields the dissipation due to slip along four sets:

$$\bar{w} = (\sigma_1 - \sigma_3) + (\sigma_2 - \sigma_3)k \tag{12}$$

where $\bar{w} = 4w/e_1$.

Rewriting eqs. 9 and 12 yields:

$$(\sigma_1 - \sigma_3)\left[N_1S_1(1 + Rk) - \tan\phi\left(N_1^2 + RN_2^2\right)\right] = C + \tan\phi\sigma_3 \tag{13a}$$

and:

$$(\sigma_1 - \sigma_3)(1 + Rk) = \bar{w} \tag{13b}$$

where $R = (\sigma_2 - \sigma_3)/(\sigma_1 - \sigma_3)$ is the stress ratio. These equations express the dependence of the stress difference $(\sigma_1 - \sigma_3)$, the stress ratio R and the dissipation $\bar{w}$ on the fault orientation N_1 and N_2 for given friction angle ϕ, cohesion C and strain ratio k. Equation 13a can be satisfied by many fault orientations N_1 and N_2, each with its corresponding stress. Similarly, any stress conditions will provide a solution to eq. 13b.

Assumption: There are faults which minimize simultaneously the stress difference $(\sigma_1 - \sigma_3)$ in eq. 13a and the dissipation $\bar{w}$ in eq. 13b. It is further assumed that these faults would *slip preferentially*. In other words, some faults have such orientations which require smaller stresses and dissipation, and thus, these faults are likely to slip before the others. These faults are called here the *preferred faults*.

The preferred faults and the corresponding stress conditions, have been determined numerically from eqs. 13. The solution procedure is the following:

(1) Material properties, ϕ and C, strain ratio k, and normalized confining pressure $P = \sigma_3/(\sigma_1 - \sigma_3)$ are chosen.

(2) A search is conducted for the combination of N_1, N_2 and R which minimize $(\sigma_1 - \sigma_3)$ in eq. 13a for the conditions chosen in (1). The complete range, namely, $1 \geqslant N_1 \geqslant 0$, $1 \geqslant N_2 \geqslant 0$ and $R \geqslant -0.5$ is searched.

(3) A two stage search is conducted for the combination of N_1, N_2 and R which minimize $\bar{w}$ (eq. 13b). First, the stress difference $(\sigma_1 - \sigma_3)$ is calculated by substituting N_1, N_2, R, ϕ, C, k and P into eq. 13a (note that eq. 13a must be satisfied). Then, the parameters $(\sigma_1 - \sigma_3)$, k and R are substituted into eq. 13b.

In the present model we have considered only the deformation associated with slip along faults. However, the blocks bounded by the faults are also distorted elastically. The strain energy of distortion, w_d, is also calculated here for comparison. By assuming homogeneous stress distribution, the distortion energy per unit volume is (after Jaeger and Cook, 1969):

$$w_d = \frac{1}{12G}\left[(\sigma_1 - \sigma_2)^2 + (\sigma_2 - \sigma_3)^2 + (\sigma_3 - \sigma_1)^2\right] \tag{13c}$$

where G is the elastic shear modulus. Similarly to the dissipation $\bar{w}$, (eq. 13b), the strain distortion energy is minimized for certain fault orientations. These orientations and the associated stress ratios R, are calculated in two stages. First, the stress difference $(\sigma_1 - \sigma_3)$ is calculated by substituting N_1, N_2, R, ϕ, C, k and P into eq. 13a, the slip criterion. Then, the parameters $(\sigma_1 - \sigma_3)$ and R are substituted into eq. 13c. A search is conducted to those parameters which minimize w_d for a constant shear modulus G.

The results of these numerical calculations with some experimental data are shown in Fig. 3. The stress ratios R, which minimize the *stress difference* $(\sigma_1 - \sigma_3)$ in eq. 13a are shown in a solid line (Fig. 3). The stress ratio varies in steps, $R = 0$ for all $k < 0$, and $R = 1$ for all $k > 0$; this result is independent of the confining pressure P. The stress ratios R, which minimize the *dissipation* (eq. 13b) are shown in dotted line for $P = 0$ (Fig. 3a) and for $P = 0.15$ (Fig. 3b). Finally, the stress ratios R for which the strain energy of distortion, w_d, is minimized, are shown in dashed line for $P = 0$ (Fig. 3a) and $P = 0.10$ (Fig. 3b).

The stress ratios R which minimize $(\sigma_1 - \sigma_3)$, $\bar{w}$ or w_d deviate significantly for most strain ratios under unconfined conditions of $P = 0$, where $P = \sigma_3/(\sigma_1 - \sigma_3)$ (Fig. 3a). On the other hand, the stress ratios which minimize $(\sigma_1 - \sigma_3)$, $\bar{w}$ or w_d, become very similar to each other for $P \geqslant 0.10$ (Fig. 3b).

The numerical solutions presented in Fig. 3 indicate two main results:

(1) For confined cases ($P \gtrsim 0.15$), there are faults which minimize simultaneously the stress difference $(\sigma_1 - \sigma_3)$ and the dissipation $\bar{w}$, confirm the assumption made above. Furthermore, the strain distortion energy is also minimized for these faults (Fig. 3b).

(2) *Axisymmetric* stresses ($R = 0$ or $R = 1$) minimize both the stress difference necessary for slip and the dissipation under *three-dimensional* strain ($k \neq 0$). For the cases of $\sigma_3/(\sigma_1 - \sigma_3) \gtrsim 0.15$ the solution of eqs. 13a and 13b coincide to give:

$$\sigma_1 = \sigma_2 \text{ for } k \geqslant 0 \tag{14a}$$

and:

$$\sigma_2 = \sigma_3 \text{ for } 0 \geqslant k \geqslant -0.5 \tag{14b}$$

For plane strain the intermediate stress σ_2 is bounded by

$$\sigma_1 \geqslant \sigma_2 \geqslant \sigma_3 \text{ for } k = 0 \tag{14c}$$

The derivation of axisymmetric stresses (Fig. 3 and eqs. 14) for three-dimensional strain requires some discussion. At first this result opposes intuition: three-dimensional strain would require three-dimensional stress. A careful examination of the assumptions of the proposed model resolves this apparent contradiction. It was

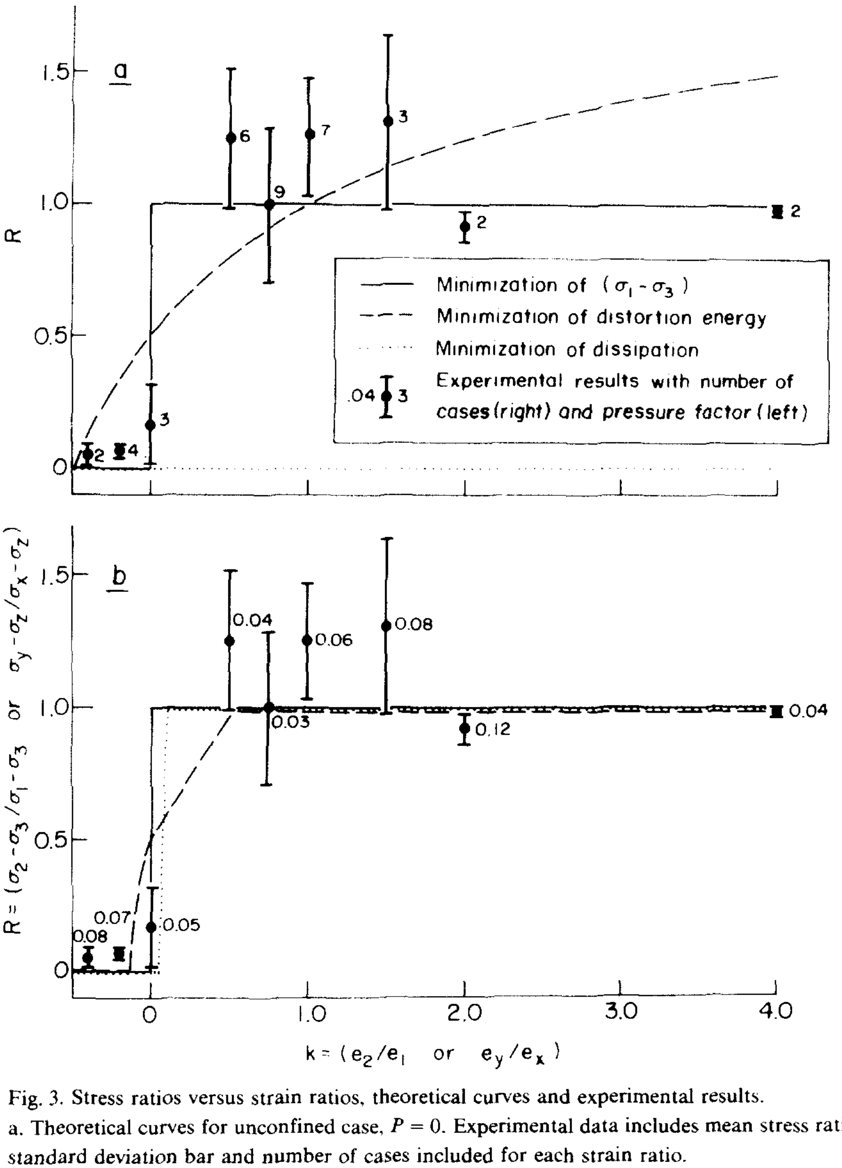

Fig. 3. Stress ratios versus strain ratios, theoretical curves and experimental results.
a. Theoretical curves for unconfined case, $P = 0$. Experimental data includes mean stress ratio (solid dot), standard deviation bar and number of cases included for each strain ratio.
b. Theoretical curves for confined cases of $P = 0.15$, and experimental confining factors P.

assumed that the preferred faults minimize the stress difference in the slip equation (eq. 13a) and minimize the dissipation (eq. 13b), while simultaneously, these faults satisfy the applied three-dimensional strain field. The kinematic analysis of slip along faults indicates that *four* sets, which do not include the three principal stress axes, are necessary to accommodate three-dimensional strain (Reches, 1978; eq. 1

above). On the other hand, the well known derivation for faults, which minimize the stress difference, $\sigma_1 - \sigma_3$, yields *two* sets which include the σ_2 axis (e.g. Jaeger and Cook, 1969). However, an axisymmetric stress generates an infinite number of sets of faults which require the *same* stress difference, $\sigma_1 - \sigma_3$. The preferred faults are among these many sets; but the preferred faults are the only ones which can accommodate the applied strain field under the given stress difference with minimum dissipation.

The orientations of the preferred faults can be derived through an analytical solution for three special cases. Case I is for $k = 1$, namely $e_1 = e_2$. This is the "extension" experiment in a triaxial test. Therefore, due to symmetry:

$$_{\mathrm{I}}N_1 = {}_{\mathrm{I}}N_2,\ {}_{\mathrm{I}}\sigma_1 = {}_{\mathrm{I}}\sigma_2 \tag{15a}$$

and:

$$_{\mathrm{I}}S_1 = \left(\frac{1 - 2\,_{\mathrm{I}}N_1^2}{2}\right)^{1/2} \qquad \text{(after eq. 5)} \tag{15b}$$

Case II is for $k = 0$, namely $e_2 = 0$. This is the plane strain experiment. Obviously:

$$_{\mathrm{II}}N_2 = 0 \tag{16a}$$

and also:

$$_{\mathrm{II}}S_1 = \left(1 - {}_{\mathrm{I}}N_1^2\right)^{1/2} \qquad \text{(after eq. 5)} \tag{16b}$$

Case III is for $k = -0.5$, namely $e_2 = e_3$, which is the "compression" experiment in triaxial tests. Therefore, due to symmetry:

$$_{\mathrm{III}}N_2 = {}_{\mathrm{III}}N_3,\ {}_{\mathrm{III}}\sigma_2 = {}_{\mathrm{III}}\sigma_3 \tag{17a}$$

and also:

$$_{\mathrm{III}}N_1 = 1 - 2\,_{\mathrm{III}}N_2 \qquad \text{(after eq. 4b)} \tag{17b}$$

and:

$$_{\mathrm{III}}S_1 = \left(1 - {}_{\mathrm{III}}N_1^2\right)^{1/2} \tag{17c}$$

Substituting conditions (15), (16) and (17) into eqs. 9 and 12 yields:

$$2\left({}_{\mathrm{I}}\sigma_1 - {}_{\mathrm{I}}\sigma_3\right)\left[{}_{\mathrm{I}}N_1\left(\frac{1 - 2\,_{\mathrm{I}}N_1^2}{2}\right)^{1/2} - \tan\phi N_1^2\right] = \bar{C} \tag{18a}$$

$$2\left({}_{\mathrm{I}}\sigma_1 - {}_{\mathrm{I}}\sigma_3\right) = {}_{\mathrm{I}}\bar{w} \tag{18b}$$

$$\left({}_{\mathrm{II}}\sigma_1 - {}_{\mathrm{II}}\sigma_3\right)\left[{}_{\mathrm{II}}N_1\left(1 - {}_{\mathrm{II}}N_1^2\right)^{1/2} - \tan\phi N_1^2\right] = \bar{C} \tag{19a}$$

$${}_{\mathrm{II}}\sigma_1 - {}_{\mathrm{II}}\sigma_3 = {}_{\mathrm{II}}\bar{w} \tag{19b}$$

$$\left({}_{\mathrm{III}}\sigma_1 - {}_{\mathrm{III}}\sigma_3\right)\left[{}_{\mathrm{III}}N_1\left(1 - {}_{\mathrm{III}}N_1^2\right)^{1/2} - \tan\phi N_1^2\right] = \bar{C} \tag{20a}$$

and:

$$ {}_{III}\sigma_1 - {}_{III}\sigma_3 = {}_{III}\bar{w} \tag{20b} $$

respectively. In these three pairs of equations, the dissipation $\bar{w}$ depends only on $\sigma_1 - \sigma_3$. Therefore, the faults that minimize $\sigma_1 - \sigma_3$ in eqs. 18a, 19a and 20a will also minimize the dissipation $\bar{w}$ in eqs. 18b, 19b and 20b, respectively. Solving eqs. 18a, 19a and 20a for a N_1 that minimizes $\sigma_1 - \sigma_3$ at constant $\bar{C}$ yields the following:

Case I

$$ \begin{aligned} {}_{I}N_1 &= \tfrac{1}{2}(1 - \sin\phi)^{1/2} \\ {}_{I}N_2 &= {}_{I}N_1 \\ {}_{I}S_1 &= \tfrac{1}{2}(1 + \sin\phi)^{1/2} \end{aligned} \tag{21} $$

Case II

$$ \begin{aligned} {}_{II}N_1 &= (\sqrt{2}/2)(1 - \sin\phi)^{1/2} \\ {}_{II}N_2 &= 0 \\ {}_{II}S_1 &= (\sqrt{2}/2)(1 - \sin\phi)^{1/2} \end{aligned} \tag{22} $$

Case III

$$ \begin{aligned} {}_{III}N_1 &= (\sqrt{2}/2)(1 - \sin\phi)^{1/2} \\ {}_{III}N_2 &= \tfrac{1}{2}(1 + \sin\phi)^{1/2} \\ {}_{III}S_1 &= (\sqrt{2}/2)(1 + \sin\phi)^{1/2} \end{aligned} \tag{23} $$

respectively. The minimal stress difference $\sigma_1 - \sigma_3$ is derived by substituting eqs. 21, 22 and 23 into eqs. 18a, 19a and 20a. This difference is the *same* for all three cases:

$$ \sigma_1 - \sigma_3 = 2\bar{C}\frac{\cos\phi}{1 - \sin\phi} \tag{24} $$

The intermediate stress, σ_2, is different in the three cases:

$$ \begin{aligned} &{}_{I}\sigma_2 = {}_{I}\sigma_1 \\ &{}_{II}\sigma_3 \leqslant {}_{II}\sigma_2 \leqslant {}_{II}\sigma_1 \\ &{}_{III}\sigma_2 = {}_{III}\sigma_3 \end{aligned} \tag{25} $$

The analytical results of the three special cases (eqs. 21–25) are identical to the results of the numerical calculations for the minimization of $\sigma_1 - \sigma_3$ and $\bar{w}$ (for $P \gtrsim 0.15$).

The orientations of the preferred faults were determined numerically for all strain ratios, and analytically for the three special cases. By comparing the numerical and analytical orientations of the preferred faults for the three special cases, we found that the orientations of the preferred faults for *all* cases can be represented by the following expressions:

$$
\left.
\begin{aligned}
N_1 &= \frac{1}{2}\left(\frac{2}{1+k}\right)^{1/2}(1-\sin\phi)^{1/2}\\
N_2 &= \frac{1}{2}\left(\frac{2k}{1+k}\right)^{1/2}(1-\sin\phi)^{1/2}\\
N_3 &= (\sqrt{2}/2)(1+\sin\phi)^{1/2}\\
S_1 &= \frac{1}{2}\left(\frac{2}{1+k}\right)^{1/2}(1+\sin\phi)^{1/2}\\
S_2 &= \frac{1}{2}\left(\frac{2k}{1+k}\right)^{1/2}(1+\sin\phi)^{1/2}\\
S_3 &= (\sqrt{2}/2)(1-\sin\phi)^{1/2}
\end{aligned}
\right| \qquad (26)
$$

for $k \geqslant 0$. The orientations of the preferred faults for $-0.5 \leqslant k \leqslant 0$ are:

$$
\left.
\begin{aligned}
N_1 &= (\sqrt{2}/2)(1-\sin\phi)^{1/2}\\
N_2 &= (\sqrt{2}/2)|k|^{1/2}(1+\sin\phi)^{1/2}\\
N_3 &= (\sqrt{2}/2)(1-|k|)^{1/2}(1+\sin\phi)^{1/2}\\
S_1 &= (\sqrt{2}/2)(1+\sin\phi)^{1/2}\\
S_2 &= (\sqrt{2}/2)|k|^{1/2}(1-\sin\phi)^{1/2}\\
S_3 &= (\sqrt{2}/2)(1-|k|)^{1/2}(1-\sin\phi)^{1/2}
\end{aligned}
\right| \qquad (27)
$$

Equations 26 and 27 are the orientations of fault I of the four sets (see eq. 1. By simple variations of the signs of N_i and S_i according to eq. 1, four sets of faults in orthorhombic symmetry are derived.

The loci of the poles to the predicted faults according to eqs. 26 and 27, are shown in Fig. 9.

In summary, we analyzed the accommodation of strain of an idealized model by slip along many preexisting surfaces of discontinuity which develop to become faults. It is shown that four sets of faults in orthorhombic symmetry are necessary and sufficient to accommodate three dimensional deformation. We derived a *slip criterion* (eq. 9) which indicates the stress field required for slip along the faults, in a specified material and for an applied strain field. We assume that the faults which satisfy the slip criterion, and minimize the dissipation (eq. 12) simultaneously, are the *preferred faults*. We derive the orientation of these preferred faults (eqs. 26, 27) and the stress fields required for slip along them (eqs. 14).

APPLICATIONS

In the foregoing analysis we derived the orientations of preferred sets of faults which developed in an idealized model subjected to *strain* boundary conditions. We also derived the *stresses* necessary to accommodate this strain by slip along the preferred faults. The polyaxial tests on cubic samples of sandstones, limestones and granites presented in Part I (Reches and Dieterich, 1983), were run under conditions similar to those assumed in the theoretical analysis. Thus, these experimental results will be compared with the theoretical predictions.

In these experiments we used an apparatus with three mutually perpendicular presses, two of which are servo-controlled. During the experiments the displacement rates in these two presses, designated as X and Y, were constant. The servo-control system determined the stresses necessary to maintain the fixed displacement rates, and varied the stresses accordingly. In the third press, designated as Z, the stress was maintained constant. The X, Y and Z are the principal axes of the deformation (Reches and Dieterich, 1983). Rotation was not permitted on the six faces of the rock cubes. Therefore, each sample was subjected to mixed boundary conditions: constant displacement rates along two principal axes, and constant stress along the third principal axis.

In Part I it is shown that samples of all the rock types that were subjected to three-dimensional deformation display three or four sets of faults in orthorhombic symmetry. Two out of 28 samples are presented in Fig. 4. It was also shown that due to this apparent symmetry, the poles to the faults may be rotated into one quarter of the stereonet projection (see Part I). We consider the average fault, calculated after the rotation of all experimental faults into one quarter of the stereonet, as the representative of the faults measured in the sample. Figure 5 displays the average faults in all 28 experiments. If the pole to the average fault falls on one of the principal planes, XY, XZ or YZ (e.g., experiment RD-70 in Fig. 5a), it represents a set of two faults in conjugate pattern; if however, the pole to the average fault falls between the principal planes, it represents three or four faults in orthorhombic symmetry. The circle of confidence at $\alpha = 0.05$ level (Fisher's method), ranges from 1.6° for sample RD-62 to 15.9° for RD-70, with mean value of 6.2°.

It is apparent from Fig. 5a that faults in most samples show orthorhombic symmetry as the poles to the average faults are distributed between the XZ and YZ planes. Figures 5b, c, d, e show the average faults according to rock type and experimental strain ratio, $k = e_y/e_x$. We plotted the theoretical loci of poles to the average faults, derived above (eqs. 26, 27), on the same stereonets of Fig. 5. The theoretical loci appear as a net of great and small circles on the Wulff stereonets. These circles are the graphic presentation of the two variables in eqs. 26 and 27: the friction angle ϕ and the strain ratio k. Each circle is the locus of the average fault for the constant value of the marked variable. The star symbol in Fig. 5b occurs at the intersection of the great circle of strain ratio $k = 4$ and the small circle of the friction angle 30°. According to the present analysis this symbol is the theoretical pole of the average fault in a rock sample with friction angle of 30° which failed under strain ratio of 4. One can compare now the agreement between the theoretical predictions and the experimental results.

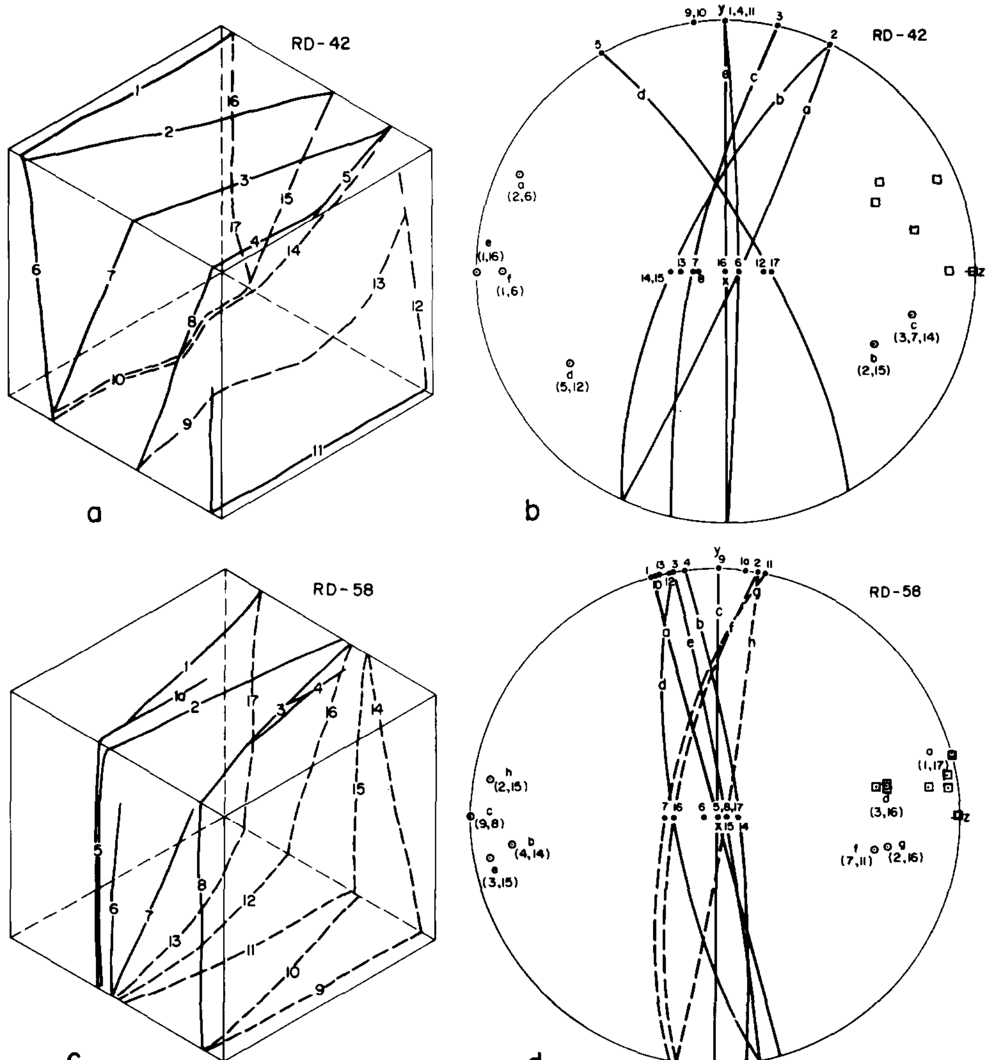

Fig. 4. The fault pattern in a Berea sandstone sample (RD-42) and a Sierra-White granite sample (RD-58) that faulted under three-dimensional strain field. On the block diagrams (a and c) fault traces are marked in a solid line on x_1, y_1 and z_1 faces and in dashed line on x_2, y_2 and z_2 faces. Traces which belong to the same fault surface are connected with a great circle on the stereographic projection on the right (b and d). The open squares in the upper right quarter of the stereographic projections are the normal to the faults rotated by orthorhombic operation. The average fault is calculated for this rotated position.

The comparison of the fault orientations

The series of experiments of Berea sandstone provide the clearest distribution in the current experimental work (Fig. 5b). The poles to the average faults in the eleven

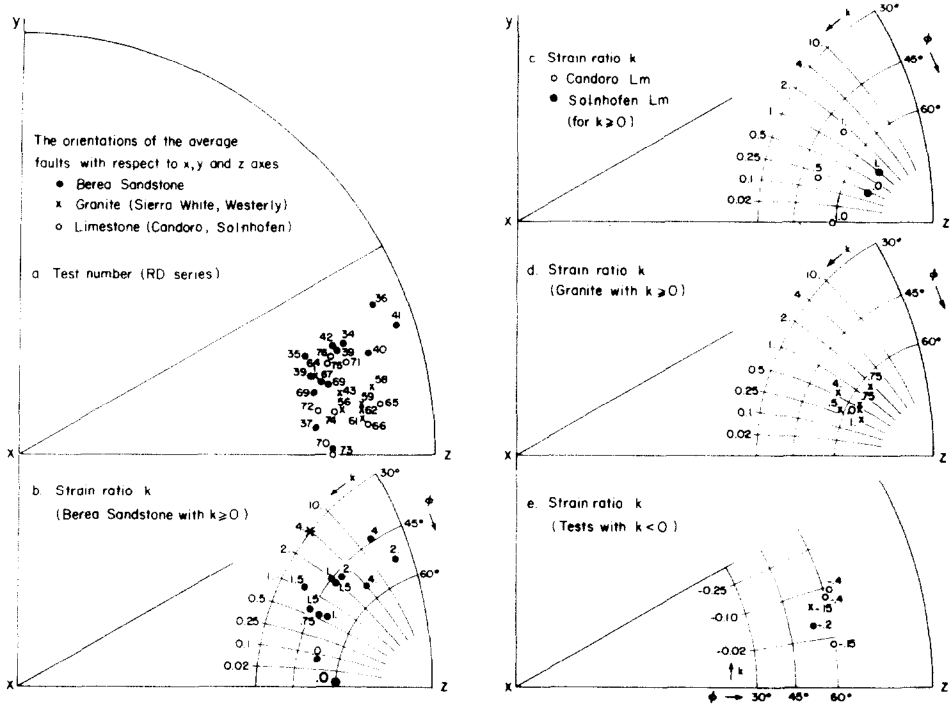

Fig. 5. The normals to the average faults of all samples plotted on a 30° section of a Wulff net. The small and great circles marked in Figures b, c, d and e are the loci of the normals to the preferred faults predicted by the slip model (eqs. 26 and 27).

samples are distributed along the small circle for $\phi = 44°$, indicating a friction angle of $44° \pm 4°$. These poles also occur in approximate agreement with the predicted strain ratios. Faults in samples of large strain ratios, $k \geqslant 2$, tend to fall into the region predicted for such large ratios, and faults of intermediate strain ratios, $2 > k \geqslant 0.5$, tend to fall in the central region. The average faults in the Candoro limestone and the Solnhofen limestone (Fig. 5c), indicate friction angles of 50° and 68° respectively. Here, too, experimental and theoretical orientations agree approximately.

The deviations of the experimental average faults of the 17 samples (Figs. 5b, c; Table I in Reches and Dieterich, 1983) from the theoretical faults, predicted by eqs. 26 and 27, were calculated. We use 44°, 50° and 68° as the friction angles for Berea sandstone, Candoro limestone and Solnhofen limestone. the deviations for the eleven samples of Berea sandstone (Fig. 5b) range from 1.0° for samples RD-38 and RD-39 to 9.4° for sample RD-41, with a mean value of 5.3°. The circle of confidence at $\alpha = 0.05$ level (Fisher's method) for these samples ranges from 2.1° for sample RD-36 to 15.9° for sample RD-70, with a mean value of 6.8°. In eight out of the eleven samples (Fig. 5b) the predicted average faults lie inside the corresponding circles of confidence. We conclude therefore, that the experimental faults in these eight samples have the predicted orientations, whereas they deviate in the other three. In all five samples of limestone (Fig. 5c) the predicted average faults lie in the corresponding circles of confidence, thus again indicating the good agreement between predicted and experimental orientations.

The granite samples display fault patterns arranged in orthorhombic symmetry, but with no apparent dependence on either the strain ratio or the friction angle (Fig. 5d). The cause for this behaviour is unknown, and will be the subject of future experiments.

The average faults in samples of negative ratios, namely when e_y is extensional, also display orthorhombic symmetry for all rock types (Fig. 5e). However, there is poor agreement between the experimental poles and the theoretical predictions. The mean deviation of the observed faults from the predicted in the four experiments of Berea sandstone and Candoro limestone is 18.3°, much larger than the circles of confidence at $\alpha = 0.05$ level.

The stresses required to maintain constant velocities in the x and y axes of the experiments, were determined continuously by the servo-control system (Reches and Doeterich, 1983). In Part I we identified three stages in most experiments: stage I of monotonously increasing stresses which terminates in the first yielding; stage II is characterized by interchange of the stresses, yielding events and general stress decrease; stage III is characterized by monotonously decreasing stresses. It was also shown that the stress ratios σ_y/σ_x, for the first yielding of all experiments, agree with the stress ratios predicted for an isotropic, homogeneous body. However, the stress ratios of the second yielding and the final stage of the experiments could not be predicted by the isotropic, homogeneous stress field.

We suggest that the first yielding represents faulting of an intact sample; whereas, the second yielding and the final stage represent strain accommodation due to slip along preexisting faults. Therefore, as the slip model is derived for preexisting faults, only the states of stress of the second yielding and final stages may be analyzed by this model. Figure 6a displays the values of σ_x (either σ_1 or σ_2) versus σ_y (either σ_2 or σ_1) for second yielding and final stage in all experiments. Equation 14a predicts that $\sigma_y = \sigma_x$ for experiments with $0 < k$ implies that σ_y is σ_1 rather than σ_x). Linear regression of the observations indicates $\sigma_y = 1.05\sigma_x + 0.1$ with $r = 0.89$ and stresses given in kbar. This is in good agreement with the predicted relationship (Fig. 3a). Figure 6b displays the values of σ_y (or σ_2) versus σ_z (or σ_3) for second yielding and final stage in all experiments with $-0.5 \leqslant k \leqslant 0$. Equation 14b predicts that $\sigma_z = \sigma_y$ for these strain ratios; linear regression indicates $\sigma_z = 0.85\sigma_z + 0.08$ with $r = 0.68$ and stresses given in kbar. This is in some agreement with the predicted relationship (Fig. 6b). Note the wider dispersion of the states of stress for $k \leqslant 0$, with respect to that for $0 < k$ (Fig. 6).

We assumed that the slip along the preferred faults minimizes simultaneously the stress difference $\sigma_1 - \sigma_3$, (eq. 13a) and the dissipation $\bar{w}$ (eq. 13a). The numerical

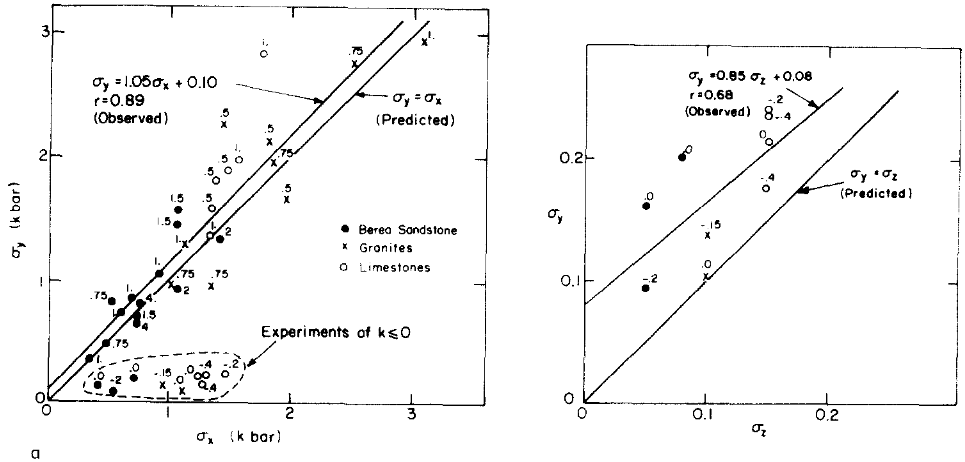

Fig. 6. a. The ratio between the two principal stresses σ_x and σ_y during second yield and final stage of all experiments. The results for experiments of $k < 0$ are encircled.
b. The ratio between the two principal stresses σ_y and σ_z during second yielding and final stage of all experiments of $k \leqslant 0$.

solution of eqs. 13 are presented for unconfined cases (Fig. 3a) and for confined cases (fig. 3b). The experimental stress ratios, $R = (\sigma_y - \sigma_z)/(\sigma_x - \sigma_z)$, are also plotted in Fig. 3 (the same data points as in Fig. 6). The mean stress ratio and the standard deviation are shown for each experimental strain ratio. The experimental data correlate reasonably well with the stress ratios predicted for the minimization of $\sigma_1 - \sigma_3$ in eq. 13a, whereas for unconfined cases, these data correlate poorly with the stress ratios predicted for the minimization of dissipation ($\bar{w}$ of eq. 13b) or strain energy of distortion [w_d of eq. 13c]. However, for confined cases, when stress ratios predicted for the three parameters $\sigma_1 - \sigma_3$, $\bar{w}$ and w_d, essentially coincide, the experimental data correlate well with the three parameters. One should note, however, that the experimental confining factor, $P = \sigma_3/(\sigma_1 - \sigma_3)$, marked in Fig. 3b, is always smaller than $P \gtrsim 0.15$ needed for the coincidence of the three parameters. Confining factors which are smaller than 0.15 will predict stress-ratios curves which are intermediate between Fig. 3a and Fig. 3b. Best fit is obtained between the experimental stress-ratios and the predicted ones for the minimization of $\sigma_1 - \sigma_3$ (Figs. 3 and 6).

The stress invariants of the experiments provide a new, empirical criterion for faulting under three-dimensional states of stress. According to this criterion faulting occurs when:

$$J_2 = aJ_1^b \qquad (28)$$

where $J_1 = \sigma_1 + \sigma_2 + \sigma_3$ (first stress invariant), $J_2 = \sigma_1\sigma_2 + \sigma_2\sigma_3 + \sigma_3\sigma_1$ (second stress invariants) and a, b are constants of the rock. Calculating power curves of type (28) to our experimental data, provides an excellent fit of stresses during first and second yielding and final stage to the same curve (Fig. 7). Correlation coefficients are 0.96 or larger. In the present experiments b ranges from 2.14 for Berea sandstone to 2.35 for Candoro limestone, and a ranges from 0.15 for Candoro limestone to 0.23 for Berea sandstone. The stress invariants for the present series of experiments show no

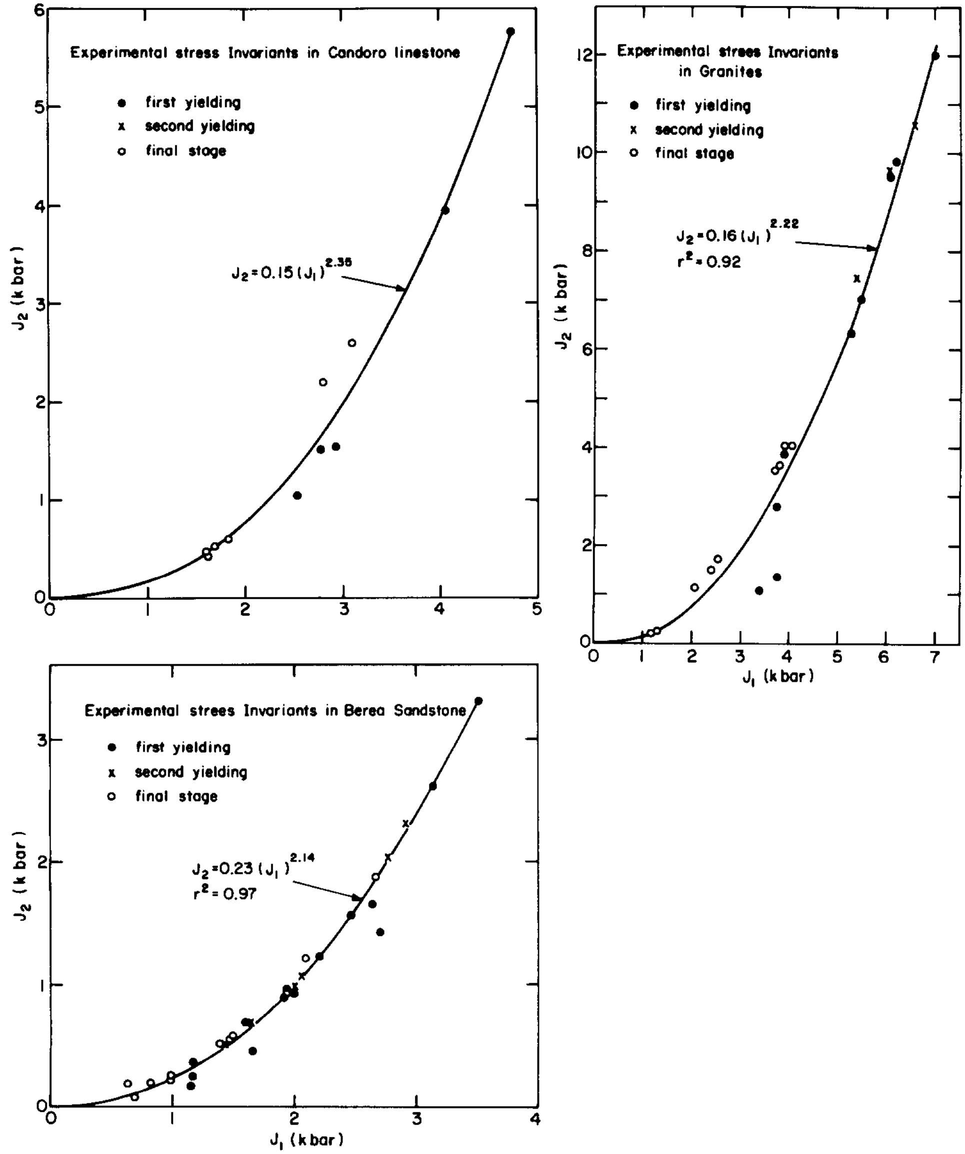

Fig. 7. The emperical relationships between the first and second stress invariants. For each rock type the stress invariants are calculated for first and second yielding and final stage.

dependence on the experimental strain ratio, or strain invariants.

The empirical criterion expressed by eq. 28 is appealing as it includes all three principal stresses and seems to represent several stages of yielding. However, we could not derive the relationship between eq. 28 and the two governing equations of the slip model, eqs. 9 and 12.

In summary, the main experimental results of part I are in agreement with the predictions of the slip model presented here. First, three or four sets of faults, in orthorhombic symmetry, developed in most samples that were subjected to three-dimensional deformation. Secondly, the orientation of the faults in samples of Berea sandstone, and Candoro and Solnhofen limestones are in good agreement with the predicted orientations for the experimental strain ratios. However, orientations of faults in granite samples and samples with $k < 0$, show no clear agreement with the predicted ones. Thirdly, the stresses in all experiments are in good agreement with the predicted stresses for slip along faults.

TABLE I

Comparison between three theories of faulting

	Anderson's model (Anderson, 1951)	Plasticity theory (e.g. Ode, 1960)	Slip model (Reches, 1978 and here)
Assumption	fault pattern reflects *local stresses*		fault pattern reflects global displacements
Boundary conditions	3-D stress	2-D displacement	3-D displacement
Internal deformation	3-D elastic strain 2-D permanent strain (implicitly)	3-D stress 2-D strain	3-D stress 3-D strain
Mechanism of deformation	elastic deformation	slip along slip surfaces (2-D strain)	slip along faults (3-D strain)
Yield criterion * on fault plane	$\tau = c + \sigma_n \tan \phi_i$	$\tau = c + \sigma_n \tan \phi_i$	$\tau = c + \sigma_n \mu$
Post failure strain	not considered	2-D strain	3-D strain
Predicted fault pattern	two sets in conjugate pattern	two sets in conjugate pattern	four sets in orthorhombic symmetry

* ϕ_i is the angle of internal friction of Navier-Coulomb yield criterion and μ is the coefficient of friction on faults planes.

CONCLUSION

The principal assumption of the slip model presented here is that strain applied on a rock is accommodated by slip along faults. The stresses which are required to maintain this slip, can be determined by specifying the resistance to slip along the faults. Furthermore, the orientations of the faults which minimize the work associated with the applied strain, can be derived.

The principal assumption of Anderson's (1951) model of faulting as well as other models (e.g. Jaeger and Cook, 1969), is that an unfaulted rock can support stresses up to a measureable maximum value. This value may be defined *locally*; for example, the stresses on a potential fault surface (Anderson, 1951), or the stresses at the corners of a tiny flaw (Griffith, 1924). This maximum value may also be defined *globally*, and then it is known as the yield criterion in the theory of plasticity (e.g. Ode, 1960). The plastic strain associated with faulting is either ignored (Anderson's

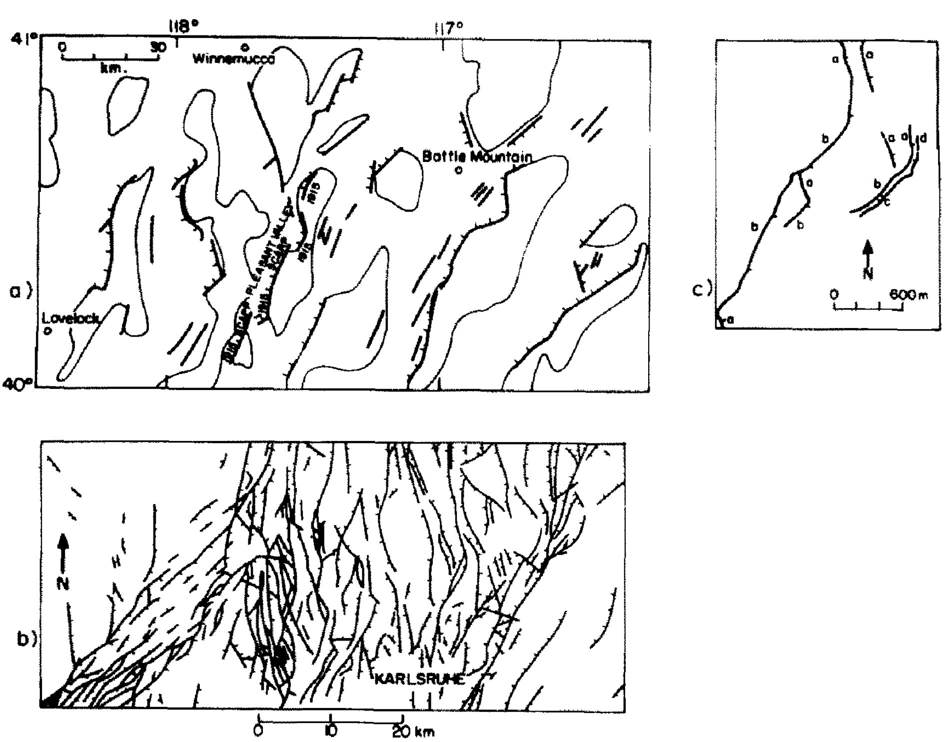

Fig. 8. A few examples of orthorhombicor "zig-zag" pattern of normal faults in extension regions. Small bars indicate downthrown blocks.

a. Recent fault scarps in Nevada. Note the crooked trace of several faults (after Wallace, 1978).

b. The fault pattern in a segment of the Rhein graben, Germany (after Illies, 1977).

c. Recent fault scarps in Dixie Valley, Nevada (after Thompson and Burke, 1973). Note that four orientations of faults, marked *a*, *b*, *c* and *d* can be distinguished.

model) or limited to plane strain (plasticity theories). The differences in both assumptions and predictions between the slip model, Anderson's model and plasticity are presented in Table I.

Many field studies show four sets of faults with orthorhombic symmetry (Fig. 8). Such patterns are observed from small scale faults (e.g., Aydin, 1977; Reches, 1978; Bruhn and Pavlis, 1981) to the regional "zig-zag" pattern of rift valleys (e.g., Illies, 1977; Freund and Merzer, 1976). Even fault scarps generated during a single earthquake, display a similar pattern (Fig. 8a, c). These patterns of faults were explained as results of multiple phases of faulting (e.g., Anderson, 1951) or as being due to preexisting basement faults. However, in some cases the *penecontemporaneous* development of three or four sets of faults is either evident or very probable (e.g., Aydin, 1977; Thompson and Burke, 1974; Bruhn and Pavlis, 1981). According to our slip model, fault patterns such as those shown in Fig. 8 can form in a *single* phase of faulting, as the effect of a three-dimensional strain field.

The main advantage of the slip model is the analysis of faulting under a three-dimensional strain field, by using a relatively simple formulation. As three-dimensional states of strain are the general cases in nature, it seems that the present analysis is an appropriate approach for the interpretation of faults in the field.

ACKNOWLEDGEMENTS

Many of the ideas presented here developed during discussions with Atilla Aydin and Gerhard Oertel. I appreciate their important contributions. Thanks to Arvid Johnson, Ray Fletcher, Andy Ruina, Jim Dieterich and the late Raphael Freund for the stimulating discussions.

Critical reviews by Atilla Aydin, Arvid Johnson, Gerhard Oertel and Dave Pollard significantly improved this paper. Thanks to Sara Fliegelmann and Yehuda Barbut for technical assistance. The experimental work presented in Part I and used here was done with the support of the U.S. Geological Survey.

APPENDIX

The orientations of faults predicted by the slip model of faulting are given in four equal area projections (Figs. 9a, b, c, d). The orientations are given as the loci of the poles to the predicted faults in the coordinate system of the principal strain axes. These projections are the solutions of eqs. 26 and 27 for various values of the strain ratio, $k = e_2/e_1$, for various friction angles, ϕ, and for various orientations of the principal strain axes.

A predicted pole to a fault is located at the intersection of the marked curve for a given strain ratio k, and the marked curve for a given friction angle ϕ. For example, the star in Fig. 5b represents the pole to the predicted fault under $k = 4$ and $\phi = 30°$.

These diagrams can be applied to determine the strain and the friction angle for

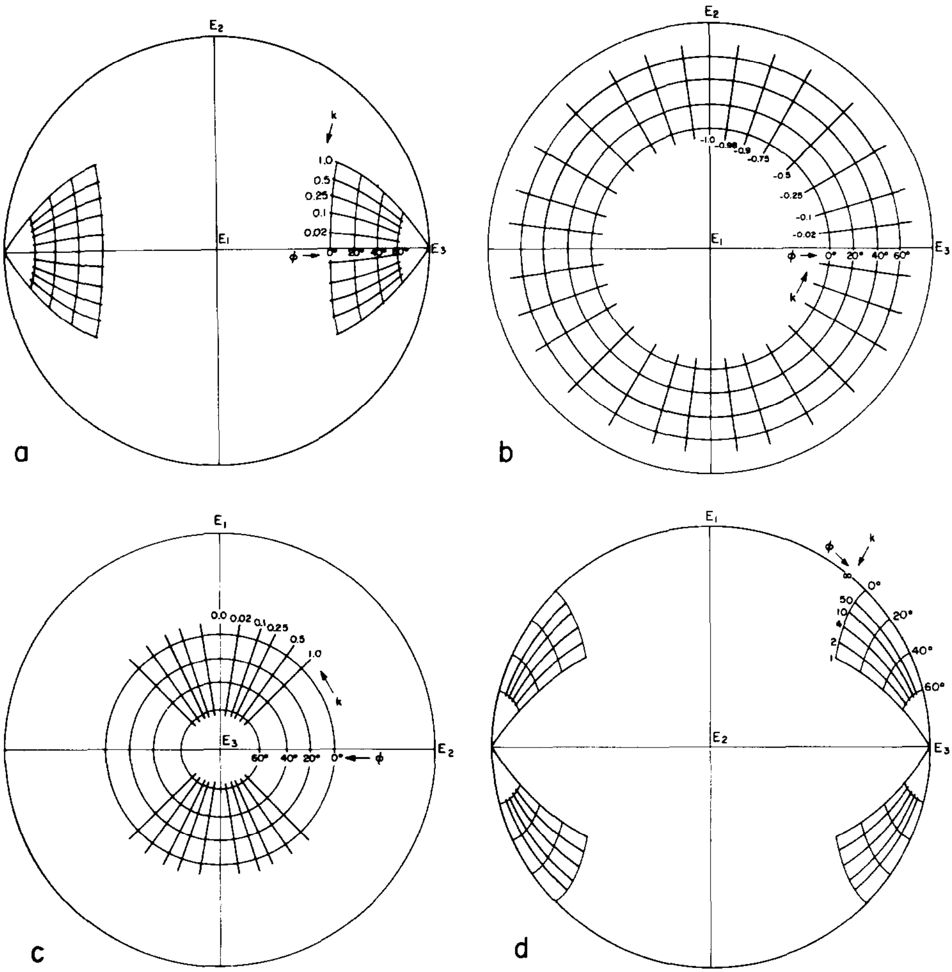

Fig. 9. Equal area projections of the faults predicted by the slip model. These are the solutions of eqs. 26 and 27. Diagrams a and b are for normal faults, diagram c is for reverse faults and diagram d for strike-slip faults. In all diagrams $k = e_2/e_1$ is the strain ratio, and ϕ is the friction angle.

field studies of faults. One should follow these steps:

(1) The poles to the faults measured in the field should be rotated to make the symmetry planes of the pattern vertical and horizontal. If many faults have been measured, their contouring will ease the analysis.

(2) The measured field data should be compared visually with the predicted diagrams (Fig. 9). The field data points, the average orientation of fault sets or the maxima of contoured projections, may fit a predicted strain ratio k, and a friction angle ϕ. We suggest that the values of k and ϕ that fit the observed data best, represent the strain during yielding and the material property respectively. Rigorous

statistical analysis may be done comparing the predicted numerical values of eqs. 26 and 27, with the measured orientations, through the common statistical techniques for oriented data (see "Applications" above).

(3) The proposed method may fail if the field measurements have no orthorhombic symmetry, or if they formed during more than one phase.

REFERENCES

Anderson, E.M., 1951. The Dynamics of Faulting. Oliver and Boyd, Edinnurgh, 206 pp.

Aydin, A., 1977. Faulting in Sandstone. Ph.D. Thesis, Stanford Univ., Stanford, Calif., 246 pp.

Bruhn, R.L. and Pavlis, T.L., 1981. Late Cenozoic deformation in the Forearc region: Matanuska Valley, Alaska: three-dimensional strain in a forearc region. Geol. Soc. Am. Bull., I, 92: 282–293.

Freund, R. and Merzer, A.M., 1976. The formation of rift valleys and their zigzag fault pattern. Geol. Mag., 133: 561–568.

Griffith, A.A., 1924. Theory and rupture. Proc. 1st Int. Congr. Appl. Mech., Delft, pp. 55–63.

Handin, J., 1969. On the Coulomb–Mohr failure criterion. J. Geophys. Res., 74: 5343–5348.

Illies, J.H., 1977. Ancient and recent rifting in the Rhinegraben. In: R.T.C. Frost, and A.J. Dikkers (Editors), Fault Tectonics in N.W. Europe. Geol. Mijnbouw, 56: 329–350.

Jaeger, J.C. and Cook, N.G.W., 1969. Fundamentals of Rock Mechanics. Methuen, London, 515 pp.

Ode, M., 1960. Faulting as a velocity discontinuity in plastic deformation. In: D. Griggs and J. Handin (Editors), Rock Deformation. Geol. Soc. Am., Mem., 79: 293–321.

Oertel, G., 1965. The mechanism of faulting in clay experiments. Tectonophys., 2: 343–393.

Paterson, M.S., 1978. Experimental Rock Deformation —The Brittle Field. Springer, Heidelberg, 254 pp.

Reches, Z., 1978. Analysis of faulting in three-dimensional strain field. Tectonophysics, 47: 109–129.

Reches, Z. and Dieterich, J., 1983. Faulting of rocks in a three-dimensional strain field. I. Failure of rocks in polyaxial, servo-control experiments. Tectonophysics, 95: 111–132.

Taylor, G.I., 1938. Plastic strain in metals. J. Inst. Met., 62: 307–324.

Thompson, G.A. and Burke, D.B., 1974. Rate and direction of spreading in Dixie Valley, basin and range province, Nevada. Geol. Soc. Am. Bull., 84: 627–632.

Wallace, R.E., 1978. Geometry and rates of change of fault-generated range fronts, north-central Nevada. J. Res., U.S. Geol. Surv., 6: 637–650.